Strojniški vestnik - Journal of Mechanical Engineering 69(2023)3-4, 100-118
DOI:10.5545/sv-jme.2022.396
Original Scientific Paper
Received for review: 2022-10-02
Received revised form: 2023-01-19
Accepted for publication: 2023-02-14

Inverse Curves - Research on Two Quondam Inversor Mechanisms

Alina Duta[1,*] – Iulian Popescu[2] – Ionut Daniel Geonea[1] – Simona-Mariana Cretu[1] – Ludmila Sass[1] – Dragos-Laurentiu Popa[1]

[1] University of Craiova, Faculty of Mechanics, Romania
[2] Academy of Technical Sciences, Romania

The field of research considered in this work is that of mechanisms generating inverse curves. We were motivated to approach this field, proposing variants of mechanisms based on Artobolevsky's inversor, in blocking conditions, due to the lack of recent applications related to inversor mechanisms that draw curves other than straight lines. Based on Crawford's inversor, Artobolevsky's inversor is structurally and kinematically analysed in what follows. Hence, we carried out the kinematic analysis and simulation of four inversor mechanisms derived from Artobolevsky's inversor, which draw different initial curves (a circle, a straight line, an ellipse and an Archimedes' spiral) were performed. Inverse curves were generated under limited operating conditions due to geometrical dimensions and kinematic parameters. Given the researchers' increasing interest in the development of applications related to inversor mechanisms (in fields such as: robotics, machine tools, visual arts and symbolic languages), as well as expanding databases of planar and spatial mechanisms, it is suggested that there is a need to create new mechanisms similar to those studied in this paper and to analyse their mode of operation.

Keywords: inversor mechanism, kinematic analysis, blocking positions

Highlights

- *Design and computational kinematic analysis of four new mechanisms that can be applied in current fields (e.g., lifting-lowering systems, conveyor belts, tool machines, suspension for electric wheels, walking and climbing robots, mechanisms for generating curves, gripping arms, kinetic light art).*
- *Addressing a topical area that is less studied but of interest to researchers.*
- *Establishing the conditions to avoid blocking with regard to the proposed inversor mechanisms.*
- *Computational kinematics analysis that identified the mechanisms used for fast movements.*

0 INTRODUCTION

Current challenges faced by researchers in various fields of Engineering can be supported by historical knowledge in the field of mechanisms and machines [1]. Attention is increasingly being paid to the creation and updating of databases containing information in various forms (text, image or diagram) in the field of planar and spatial mechanisms, including those generating curves. DMG Lib and thinkMOTION are examples of such databases [2].

In [1], several historical mechanisms for generating various curves are presented; their usefulness in a wide range of domains from engineering to the creation of new symbolic languages is highlighted. Among the mechanisms for generating curves, inversor mechanisms have been challenging specialists ever since. Two types of inversor mechanisms can be distinguished: some that direct the kinematic element in a forward-backward motion, and others in which one point moves along a given curve while another point describes an imposed curve, called the inverse curve.

For the mathematical definition of inverse curves, one should consider two curves given by polar coordinates. In Fig. 1, curve 1 is given by r_1, α and curve 2 is given by r_2, γ; P is the inversion centre of the inverse curves and β is the constant angle between r_1 and r_2.

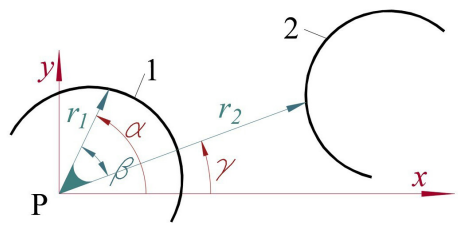

Fig. 1. *Inverse curves*

These curves are inverse to each other if Eq. (1) is verified [3].

$$r_1 \cdot r_2 = k^2, \tag{1}$$

where k is a positive number.

The inverse curves were first systematically investigated in 1824 by Steiner [4].

*Corr. Author's Address: University of Craiova, Craiova, 200512, Romania, alina.duta@edu.ucv.ro

Tables with the given direct curve / inverse curve are given in [3] (e.g., line/circle, Archimedean spiral/ Archimedean spiral, cardioid/ parabola, circle/circle, Diocles's cissoid/parabola, epi spiral/rose, hyperbola/ lemniscate, logarithmic spiral /logarithmic spiral, lituus/Fermat's spiral, sinusoidal spiral/sinusoidal spiral).

The specialized literature deals with many mechanisms that reverse the movement; they are made with levers (e.g., [5] to [7]), gears (e.g., [8] and [9]) and combinations of them (e.g., [10] and [11]). In [7], Artobolevsky presents descriptions, kinematic schemes and dimensional relationships between elements for several inversor mechanisms.

Patents for many inversor mechanisms have been obtained, e.g., lever mechanisms [12] to [14], a gear mechanism [15] and a hybrid mechanism [16].

Stephenson's popular mechanism of the steam locomotive also uses the reversing motion [17]. The first mechanism to draws a exactly straight line, invented by Peaucellier in 1864, is an inversor mechanism that transforms a circular movement into an alternative linear one. These mechanisms still have various applications nowadays. For example, [18] and [19] present the generalization of Peaucellier's inversor and suggest the possibility of generalizing other inversor mechanisms.

Hart's inversor from 1874 transforms an alternative straight-line motion into another alternative rectilinear motion that is perpendicular to the initial axis [7]. Also, the Sylvester and Kempe inversors, conceived in 1874 and in 1875, respectively, represent improvements to Hart's cell.

Kinematic (e.g., [20] and [21]), kinetostatic (e.g., [22]) and dynamic analysis (e.g., [23] and [24]), synthesis studies (e.g., [20] and [25]) and different optimization types and techniques (e.g., [26] to [28]) were carried out for the inversor mechanisms. For example, a numerical method based on the mean-square minimization of the objective function [29] can be used for the kinematic synthesis of the Stephenson mechanism. Other modern methods can also be used to optimize these planar mechanisms (e.g., the genetic algorithm, approached in [28]).

Studies were also made for the inverse kinematics of the inversor mechanisms using various software tools (e.g., MATLAB/Simulink® [20]). Some studies present the connection between mathematics and mechanisms (including inversor mechanisms) as a resource for teaching mathematics (e.g., [30], [31] and [1]).

Inversor mechanisms are used in applications such as lifting-lowering systems (e.g., [12]), conveyor belts, tool machines, suspension for electric wheels (e.g., [14]), walking machines (with different numbers of legs: two [22], four [16], or six [13], [24] and [32]), climbing robots (e.g., [21]), mechanisms generating curves, gripping arms (e.g., [25], [27] and [33]), and kinetic light art (e.g., [34]).

In some cases, a mechanism with one degree of freedom was used for some robotic leg propulsion systems. It might involve one inversor mechanism (e.g., [16]) or can rely on an inversion linkage (e.g., [13]). In other cases, the mechanism of the robotic leg has several degrees of freedom and is able to describe lines and arcs with different centres of rotation (e.g., [24]).

In the field of interactive kinetic light art, in 2016, Ivo Schoofs presented a new kinetic structure, based on Peaucellier's inverted chain, i.e., the alternative form. He built it with his team on a large scale (area of 15 m × 15 m), and placed it in the Eindhoven square at 21 m height. This structure represents a special attraction for visitors who can draw their own characters [34].

Under the circumstances, we embarked upon an applied research study of other inversor mechanisms, able to draw geometric constructions in addition to lines.

In what follows we applied Crawford's mechanisms ([35] and [36]) and Artobolevsky's mechanisms ([5], [7] and [10]); four mechanisms that draw inverse curves were also studied. For the kinematic analysis and motion simulation of the studied inversor mechanisms under the imposed conditions, we used to GWBASIC®, SolidWorks® and ADAMS® software.

1 THE STUDY OF CRAWFORD'S INVERSOR

In the 18th century, starting from one relation of inverse curves, Crawford invented two inversor mechanisms: one with the inversion centre between the two inverse curves and another with it outside them ([5], [8] and [37]). A structural and kinematic analysis of the inversor mechanism with the inversion centre between the curves, which has a circle as direct curve, is presented in this paper. The kinematic scheme of Crawford's inversor is depicted in Fig. 2.

The element 2 has the form of a T-shaped lever and turns about fixed axis A which is the inversing point of the inverse curves. The element 1 has the angle CBE of 90 degrees and is connected by the rotation joint B to the element 2. The sliders 3 and 4 are connected by the rotation joint C, and the sliders 5 and 6 are connected by the rotation joint E; these

move along elements 2 and 1. For any geometry of the mechanism, the points C, A and E are collinear. When one of the points E or C moves along an arbitrary curve, the other point describes the inverse curve.

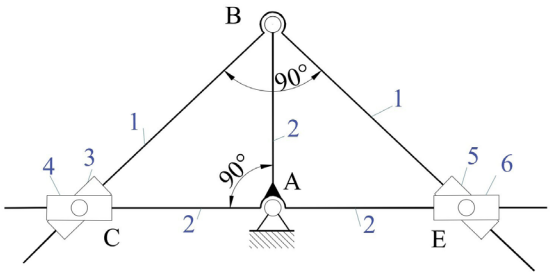

Fig. 2. *Crawford's inversor*

The mechanism performs inverse transformations because the dimensions of the mechanism verify the equation specific to inverse curves (Eq. (2)), where A is the inversion center and AC and AE are polar radii.

$$AE \cdot AC = AB^2. \tag{2}$$

The degree of mobility of this mechanism is calculated with Eq. (3), because the mechanism is not overconstrained **[38]**.

$$M = 3 \cdot n - 2C_5 - C_4, \tag{3}$$

where n is the number of mobile elements, C_5 is the number of 5th class joints, and C_4 is the number of 4th class joints.

For $n = 6$, $C_5 = 8$ and $C_4 = 0$ the value for degree of mobility is 2, i.e., two leading elements are required.

If the position of one point on a given curve is imposed, e.g., the two coordinates of point C, the point E draws the inverse curve.

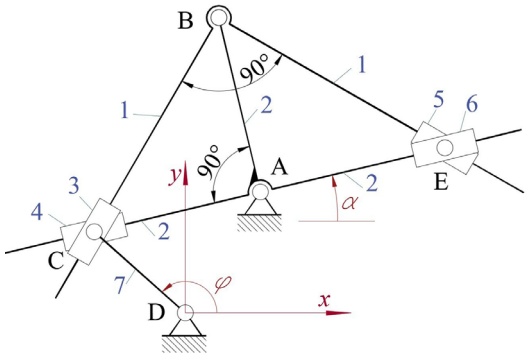

Fig. 3. *The kinematic scheme of the mechanism*

For the particular case when the direct curve is a circle, it is possible to impose the displacement of point C on it using the mechanism with the kinematic scheme from Fig. 3. The center of the circle is D and its radius equals the length of the element CD. The degree of mobility of the mechanism is equal to 1.

The structural scheme of the mechanism is depicted in Fig. 4. It can be seen that the mechanism consists of a driving element, a dyad TRT and a tetrad with 4 elements and 6 joints of the 5th class.

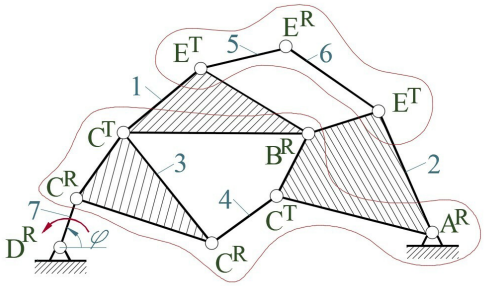

Fig. 4. *The structural scheme*

1.1 The Positions of the Mechanism

Considering as initial data DC = 31 mm, x_A = 24 mm, y_A = 29 mm, AB = 40 mm, φ = 125° and Eqs. (4) to (10), the kinematic scheme of the mechanism in GWBASIC® software was obtained (Fig. 5).

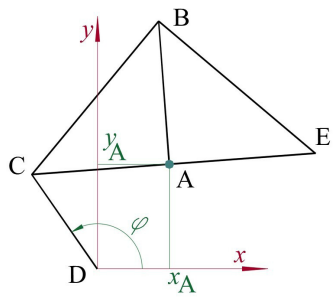

Fig. 5. *The mechanism for φ = 125 deg*

α and AC are calculated using Eq. (4).

$$\begin{cases} x_C = DC\cos\varphi = x_A + AC\cos(\alpha + \pi) \\ y_C = DC\sin\varphi = y_A + AC\sin(\alpha + \pi) \end{cases}. \tag{4}$$

Eq. (2) gives Eq. (5) that can be used to compute AE.

$$AE = AB^2 / AC. \tag{5}$$

The coordinates of B can be computed with Eqs. (6) and (7), BC is yielded by Eq. (8) and the position of E on the inverse curve is given by Eqs. (9) and (10).

$$x_B = x_A + AB\cos(\alpha + 90), \tag{6}$$

$$y_B = y_A + AB\sin(\alpha + 90), \tag{7}$$

$$BC^2 = AB^2 + AC^2, \tag{8}$$

$$x_E = x_A + AE\cos\alpha, \tag{9}$$

$$y_E = y_A + AE\sin\alpha. \tag{10}$$

For the kinematic analysis and simulation of the mechanism, the geometric model was performed in the SolidWorks® and imported into the ADAMS® software (Fig. 6).

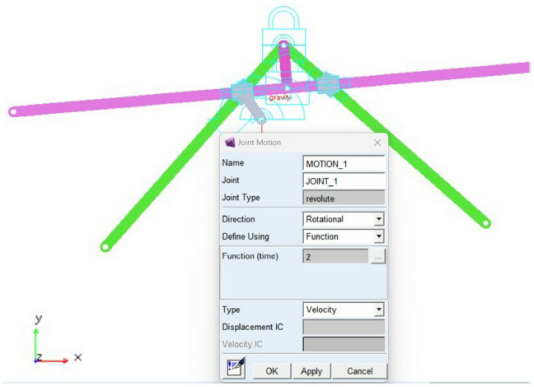

Fig. 6. *The model of the mechanism in the ADAMS® software*

1.2 Obtained Results

The rotation and translation joints were created and the motor was placed in the joint D, having angular velocity 2 rad/s (Fig. 6); taking into account the orientation of the system axes, the driving element moves in the trigonometric direction.

Fig. 7 shows the two circles drawn using the ADAMS® software: the direct curve described by point C in the trigonometric direction and the inverse one described by point E in the clockwise direction. The two circles have different areas.

The point C has uniform motion on the direct curve, its coordinates on the system axes are the trigonometric functions sine and cosine and its polar radius remains constant at 31 mm, being equal to the radius of the circle. The velocity of point C has constant modulus v = 62 mm/s and variable direction, being tangent to the trajectory. Because the velocity of the tracer point has a variable direction, it has a normal acceleration with constant modulus (Eq. (11)).

$$a^n = \omega^2 \cdot r = 124 \text{ mm/s}^2. \tag{11}$$

The inverse curve also has a circular trajectory, but, unlike the direct curve, the radius of the circle is larger; its polar radius is not constant because the center of the circle is not placed in the origin of the Cartesian system (Fig. 8b). The coordinates of the tracer point E are shown in Fig. 8a.

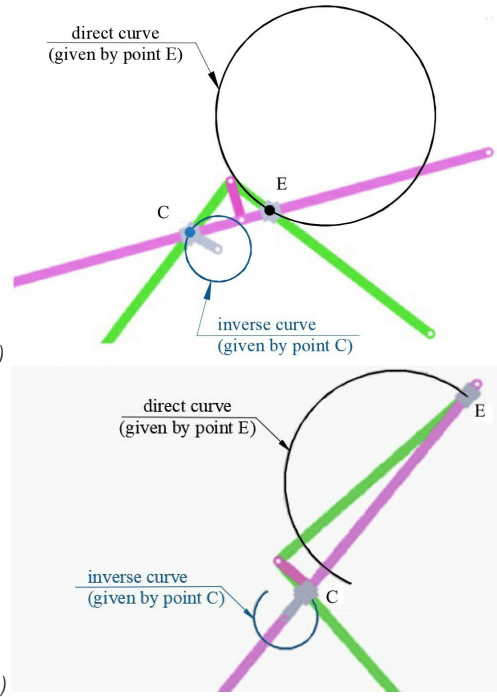

Fig. 7. *The inverse curves obtained in the ADAMS® software; a) entire curves, b) curves drawn at t = 2.5 s*

Unlike the point that draws the direct curve with uniform motion, the point that draws the reverse curve has variable motion.

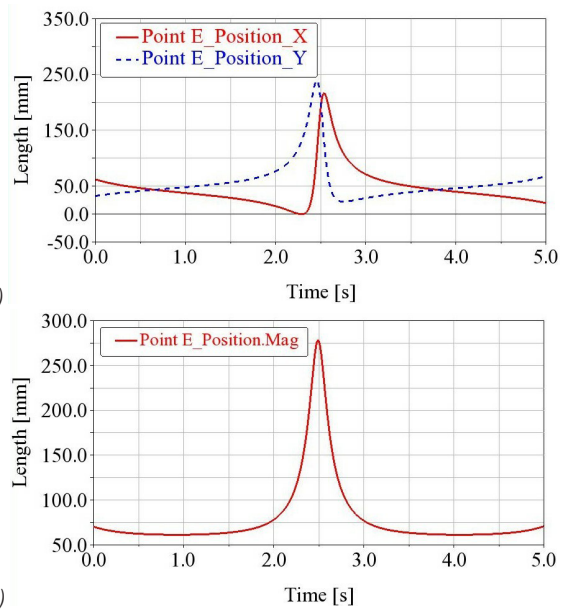

Fig. 8. *The diagram of coordinates for point E; a) the Cartesian coordinates, and b) the polar radius*

The velocity components are shown in Fig. 10a. At time t = 2.5 s, when the driving element performed

286.478 degrees from the initial position of 125 degrees (Fig. 7b), the velocity diagram of point E reveals a peak point of 2250 mm/s when the polar radius of it reaches the maximum value (Fig. 9b); because it is not a local maximum turning point of the function, the acceleration will not have the zero value and will appear as a peak point with the finite value of 45000 mm/s² (Fig. 10).

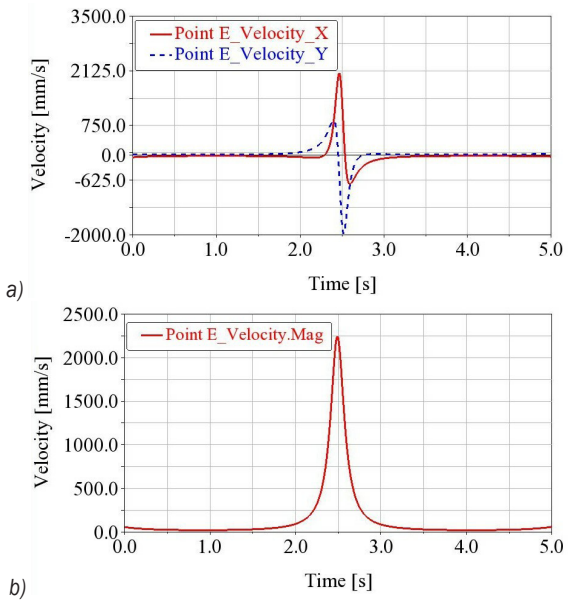

Fig. 9. *The diagram of velocity for point* E*; a) the projections on the system axes, and b) the magnitude*

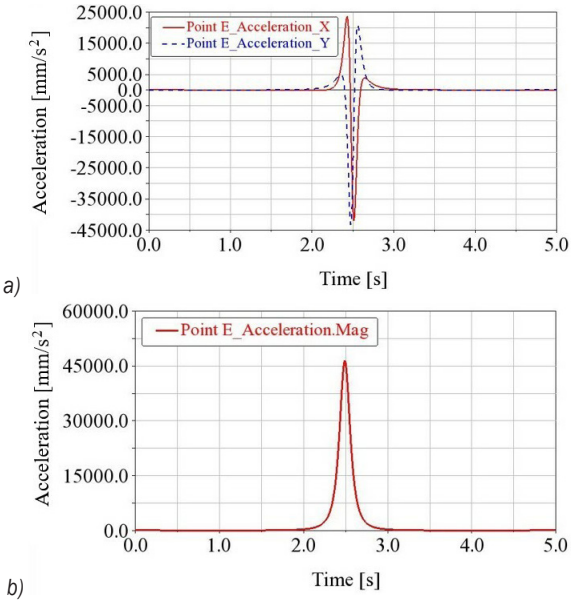

Fig. 10. *The diagram of acceleration for point* E*; a) the projections on the system axes, and b) the magnitude*

2 THE STUDY OF FOUR INVERSORS DERIVED FROM ARTOBOLEVSKY'S MECHANISM

An improvement of the Crawford's mechanism was provided by Artobolevsky (Fig. 11) [10].

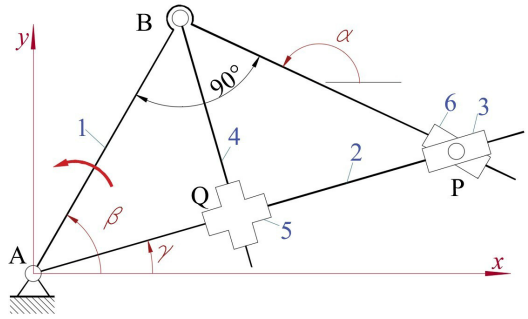

Fig. 11. *The Artobolevsky's inversor*

Our paper also focuses on the kinematic analysis and simulation of four mechanisms derived from Artobolevsky's inversor, which draw different initial curves (a circle, a straight line, an ellipse and an Archimedean spiral).

2.1 Circular Direct Curve

In order to obtain the circular trajectory of the direct curve described by point P, the rotating element CP is added to Artobolevsky's inversor mechanism (Fig. 12). The inverse curve drawn by point Q is to be found.

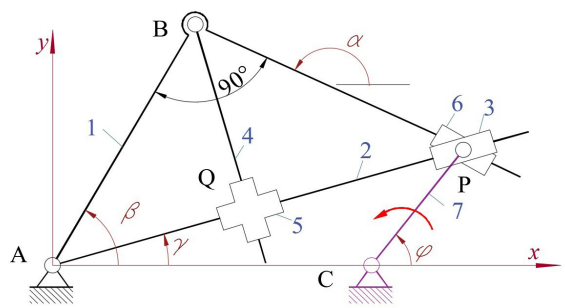

Fig. 12. *An improvement of Artobolevsky's inversor*

The equations for the position calculus are presented below (Eqs. (12) to (19)).

$$x_P = x_C + CP\cos\varphi, \tag{12}$$

$$y_P = y_C + CP\sin\varphi, \tag{13}$$

$$\begin{cases} x_B = x_P + PB\cos\alpha = AB\cos\beta \\ y_B = y_P + PB\sin\alpha = AB\sin\beta \\ \beta = \alpha - 90^0 \end{cases}, \tag{14}$$

$$AP^2 = \left(x_P - x_A\right)^2 + \left(y_P - y_A\right)^2, \quad (15)$$

$$\sin\gamma = \frac{y_P}{AP}, \quad \cos\gamma = \frac{x_P}{AP}, \quad (16)$$

$$AQ = AB^2 \,/\, AP, \quad (17)$$

$$x_Q = AQ\cos\gamma, \quad (18)$$

$$y_Q = AQ\sin\gamma. \quad (19)$$

The position of P is calculated from Eqs. (12) and (13). α, β and PB are determined from Eq. (14), and γ results from Eq. (16). The relation given by Eq. (17) is the condition of inversion and yields AQ, making possible the computation of Q's coordinates, Eqs. (18) and (19).

The initial values for the mechanism are considered as follows: x_C = 103 mm, AB = 100 mm, CP = 43 mm. Fig. 13 shows the mechanism drawn in one position with the GWBASIC® software; the given curve, drawn by the point P appears in Fig. 14, and the inverse one, drawn by the point Q is given in Fig. 15.

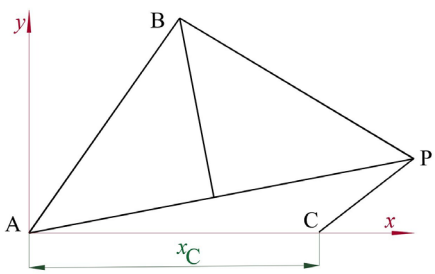

Fig. 13. *The mechanism in one position drawn with the GWBASIC® software*

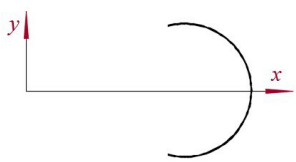

Fig. 14. *The curve drawn by point* P

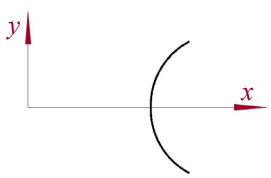

Fig. 15. *The inverse curve drawn by point* Q

The geometrical model of the mechanism it was obtained with the SolidWorks® and imported into the ADAMS® software for the kinematic analysis (Fig. 16).

After the simulation performed in ADAMS®, both direct and inverse curves were plotted. Point P does not draw a complete circle due to the dimensions of the mechanism; the arc of the circle is limited by the intersection points P_1 and P_2 between the circle drawn by point B and the circle drawn by point P (Fig. 17).

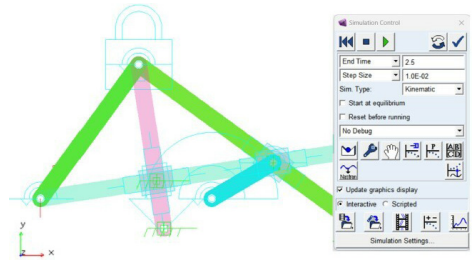

Fig. 16. *The model of the mechanism in the ADAMS® software*

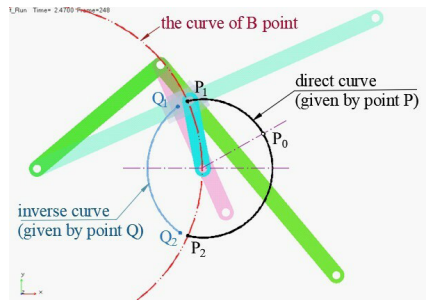

Fig. 17. *The curves drawn in the ADAMS® software*

For the mechanism from the Fig. 12, in order to avoid the operational blockage, the distance AC must be at least the sum of the radii AB and CP.

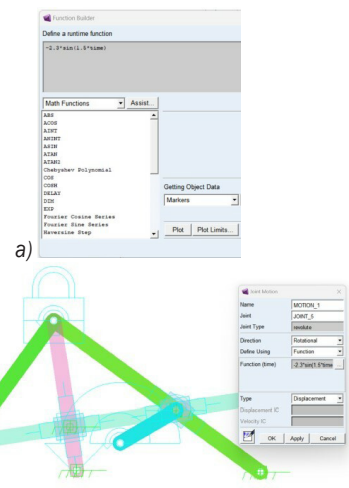

Fig. 18. *The angular motion law for driving element; a) define a runtime function, and b) the joint motion*

Since the driving element has an oscillating motion, Eq. (20) was chosen as its angular motion law in the ADAMS® software (Fig. 18).

$$f\left(time\right)=-2.3\cdot\sin\left(1.5\cdot time\right). \qquad (20)$$

The value of the driving element angle was introduced in radians in Eq. (20) and displayed in degrees (Fig. 19a). The angular velocity of the driving element is within 0 deg/s to 200 deg/s (Fig. 19b) for 2.5 s. When the driving element moves 150 degrees clockwise during one second, the point P is starting from the initial position P_0 to the P_2 point. When the driving element reaches the point P_2, it stops and changes its direction of rotation (Fig. 17).

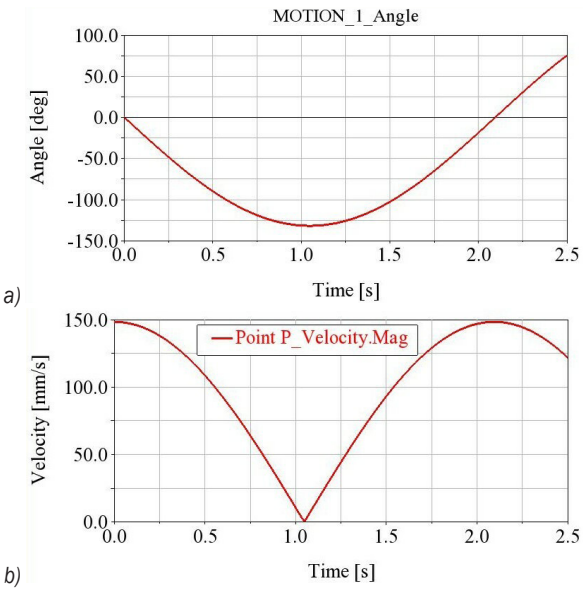

Fig. 19. *Kinematic diagrams for driving element; a) the angular position, and b) the angular velocity*

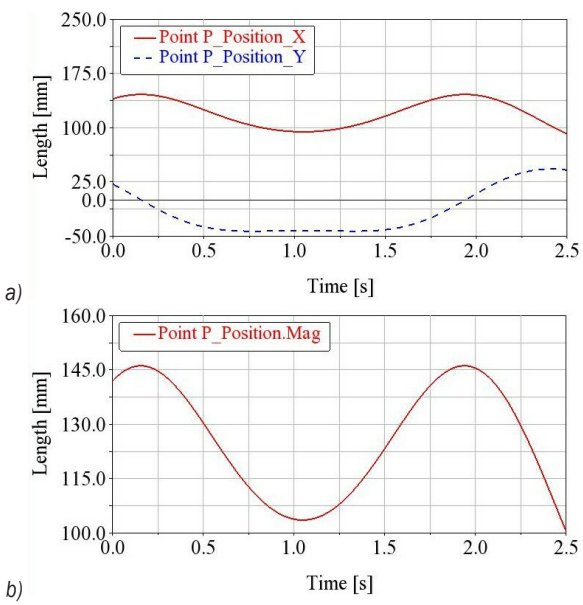

Fig. 20. *The diagram of coordinates for point* P*; a) the Cartesian coordinates; b) the polar radius*

Since the direct curve is a circular arc that does not have its centre at the origin of the Cartesian system, the polar radius is variable (Fig. 20b) and the Cartesian coordinates of the tracer point are represented in Fig. 20a.

For this law of motion, the velocity of the point P on the direct trajectory takes values between 0 mm/s and 150 mm/s (Fig. 21b) and its components on the system axes are represented in Fig. 21a.

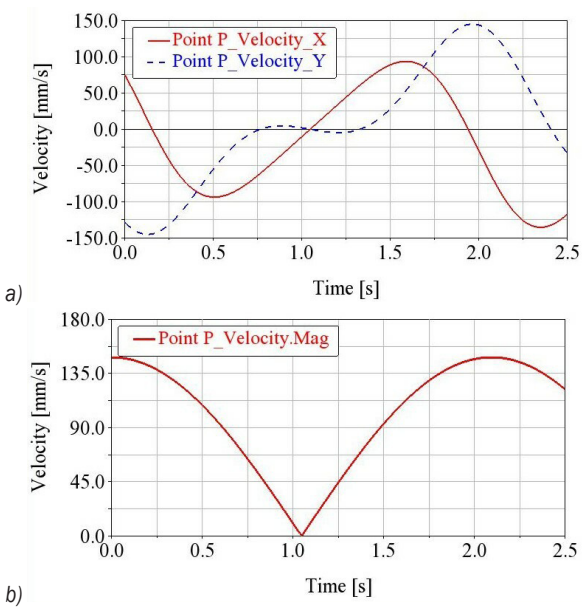

Fig. 21. *The diagram of velocity for point* P*; a) the projections on the system axes, and b) the magnitude*

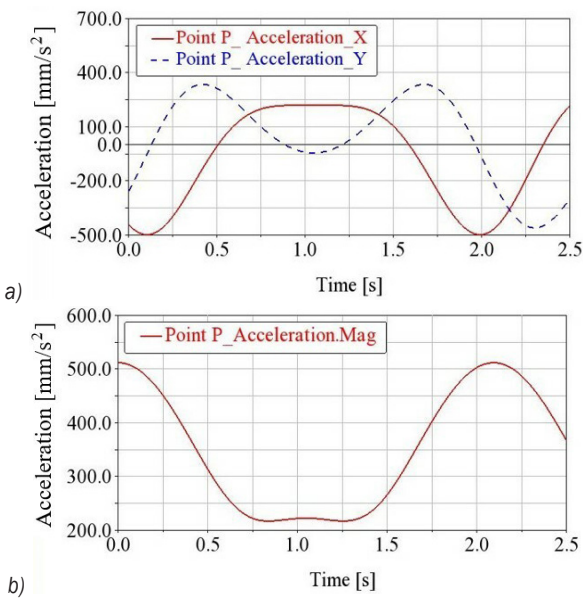

Fig. 22. *The diagram of acceleration for point* P*; a) the projections on the system axes, and b) the magnitude*

The acceleration takes values between 225 mm/s² to 520 mm/s² (Fig. 22b) and its projections on the system axes are represented in Fig. 22a.

Fig. 23 below indicates diagrams for the Cartesian coordinates and the polar radius for the inverse curve. The equations of the inverse curve are shown in the literature as functions of the direct curve variables [34]. One can check that the equation of the inverse curve is a circle, and also that its radius and centre can be determined from the ADAMS® software results. For this reason, one can consider the values of the Cartesian coordinates from the diagrams for any three points, and it is necessary to check the circle equation by them (Eq. (21)). One can determine the coordinates of the circle centre and its radius from this system of three equations and then the membership of other points to the circle can be verified.

$$\left(x_i - x_0\right)^2 + \left(y_i - y_0\right)^2 = R^2, \quad i = 1,2,3. \qquad (21)$$

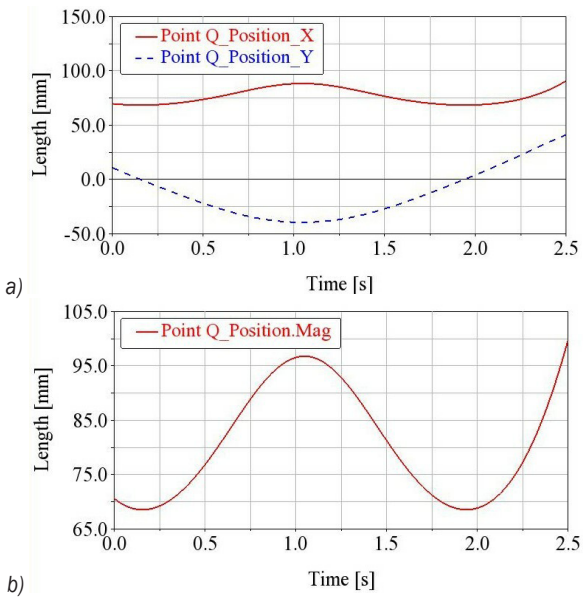

Fig. 23. *The diagram of coordinates for point Q; a) the Cartesian coordinates, b) the polar radius*

The animation and the velocity diagrams (Fig. 24) can reveal that point Q moves for one second on the inverse curve going in trigonometric direction; after stopping at point Q_2 (Fig. 17) , the direction of rotation is changed.

Fig. 24b let us conclude that the circle ensures a slow decrease of the velocity up to the moment of an imposed stop (end point P_2) for the adopted law of motion of the driving element.

At the same time, the velocity diagram of the point Q shows a portion with an approximately constant velocity of 50 mm/s, which determines the acceleration of 50 mm/s² along the corresponding interval. Due to the velocity smooth slope before stopping, the maximum acceleration does not have a peak point in the end position P_2 (Fig. 25).

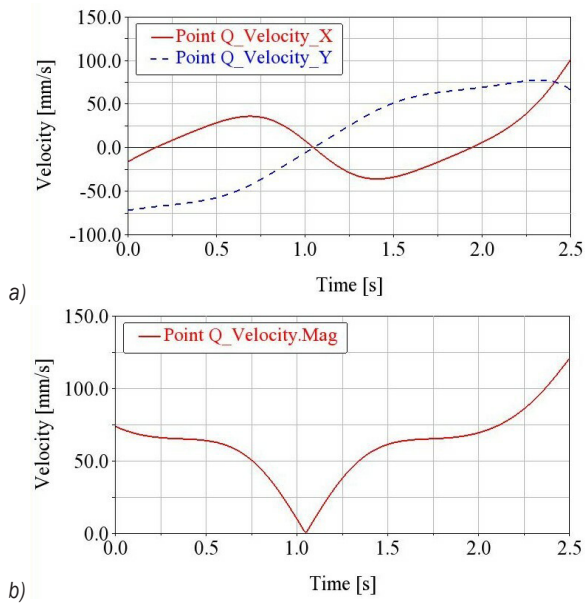

Fig. 24. *The diagram of velocity for point Q; a) the projections on the system axes, b) the magnitude*

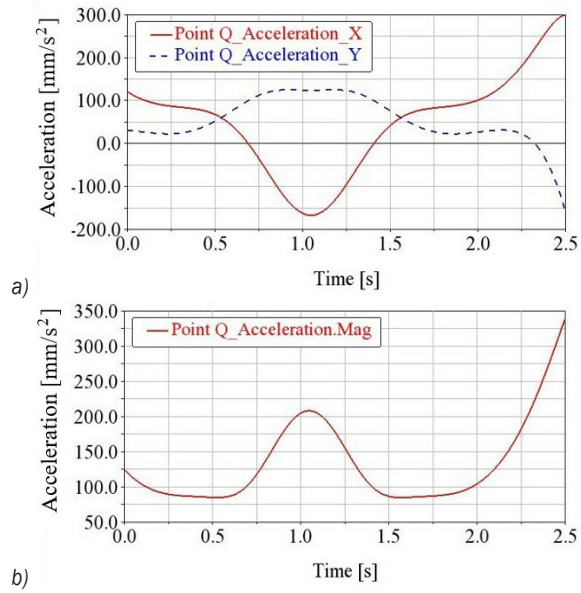

Fig. 25. *The diagram of acceleration for point Q; a) the projections on the system axes, and b) the magnitude*

2.2 Linear Direct Curve

According to the mechanism in Fig. 26, the point P has a translational motion, i.e., the direct curve is a

straight line, and the point Q plots the inverse curve. The element CP is fixed to the base and the element 7 is the driving element.

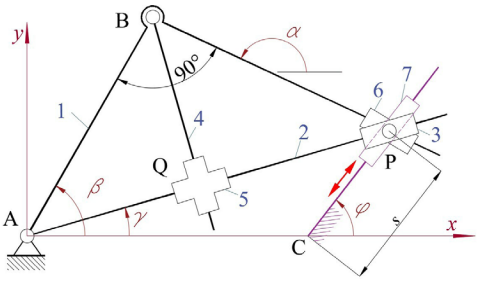

Fig. 26. *The kinematic scheme of the mechanism*

The lowest possible limit position of point P is at the intersection of the trajectory of point B with that of point P (Fig. 27).

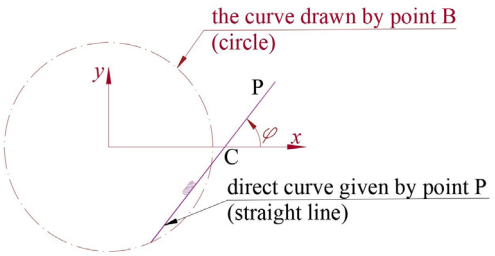

Fig. 27. *The limitation of the mechanism functioning*

In order to avoid the blockage in the operation of the mechanism (which is not caused by a change in the movement sense of the linear motor) the direction of the fixed element CP must not intersect the circular trajectory of point B.

Eqs. (22) and (23) provide the coordinates of P. For other points of the mechanism the equations are identical to those of the previously studied mechanism (Eqs. (14) to (19)).

$$x_P = x_C + S \cdot \cos\varphi, \tag{22}$$

$$y_P = y_C + S \cdot \sin\varphi. \tag{23}$$

For this mechanism, considering the same input data as those from paragraph 2.1 and φ = 30 degrees, the driving slide 7 can move on the CP guide under the abscissa axis of the reference system up to the limit point. A simulation was performed with the GWBASIC® software for an imposed stroke, S = 100 mm, in which the lower limit position of point P coincides with point C. The successive positions of the mechanism are shown in Fig. 28. A constant velocity has been considered for driving element 7, giving a variable velocity for point Q on the inverse curve.

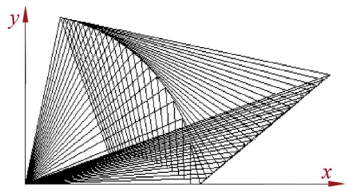

Fig. 28. *Successive positions of the mechanism*

The direct curve is plotted in Fig. 29 and the reverse curve in Fig. 30.

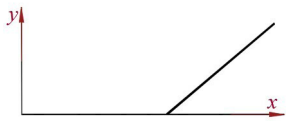

Fig. 29. *The direct curve*

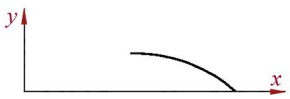

Fig. 30. *The reverse curve*

The geometrical model of the mechanism obtained with the SolidWorks® software was imported into the ADAMS® software for simulation and kinematic analysis (Fig. 31).

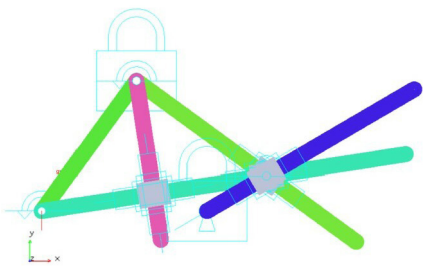

Fig. 31. *The model of the mechanism in the ADAMS® software*

A sinusoidal variation was set for the driving element 7 (Eq. (24), Fig. 32). The initial position of point P is 43 mm from C.

$$f\left(time\right) = 43 \cdot \sin\left(time\right). \tag{24}$$

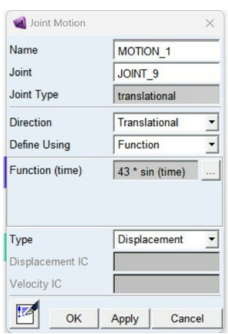

Fig. 32. *Defining runtime function in the ADAMS® software*

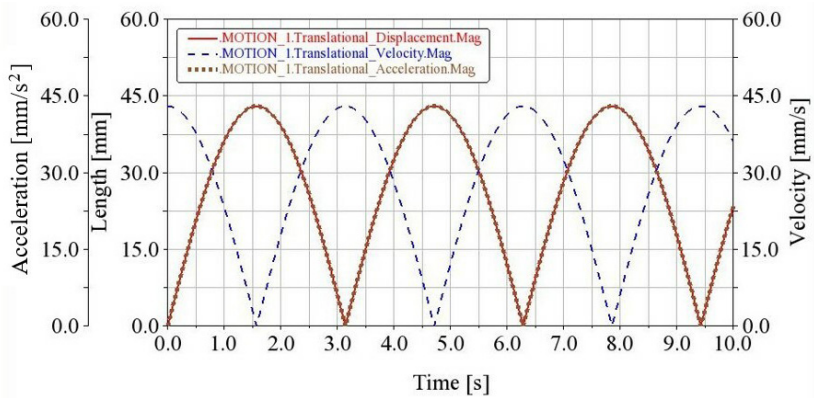

Fig. 33. *Kinematic diagrams for driving element*

The displacement [mm], the velocity [mm/s] and the acceleration [mm/s²] for driving element take values within the range of 0 to 43 (Fig. 33).

The trajectories of points P and Q were plotted during animation (Fig. 34).

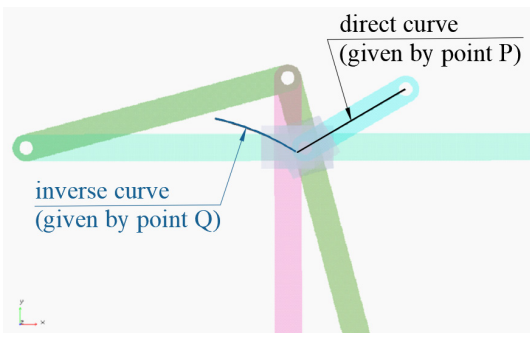

Fig. 34. *The curves drawn in the ADAMS® software*

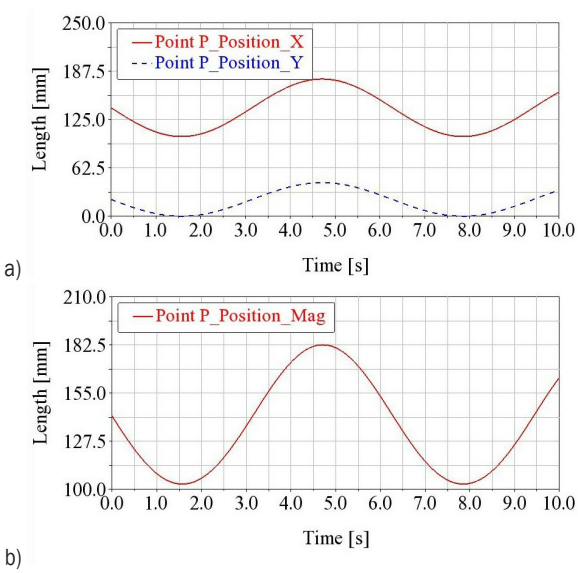

Fig. 35. *The diagram of coordinates for point P; a) the Cartesian coordinates, and b) the polar radius*

The law of P-point displacement has an inflection on both the direct and the return stroke at the middle of it.

Fig. 35 depicts the diagrams of the Cartesian coordinates and the polar radius of the point P as functions of time.

The maximum velocity has the value of 43 mm/s and the acceleration has the maximum value of 43 mm/s², in accordance with the law of motion imposed on the driving element (Figs. 36 and 37).

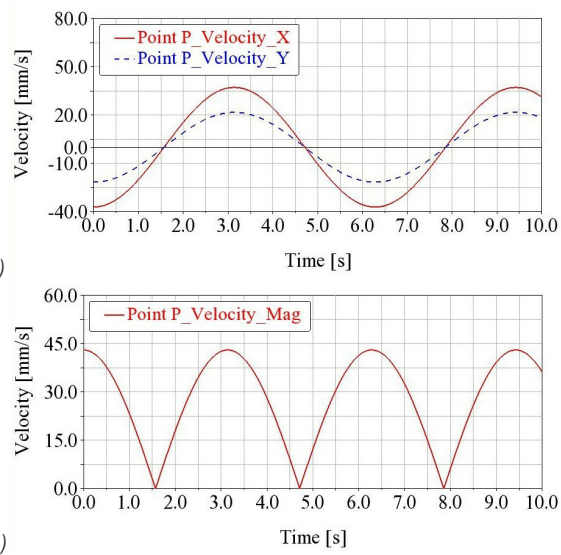

Fig. 36. *The diagram of velocity for point* P*; a) the projections on the system axes, and b) the magnitude*

The diagrams of the Cartesian coordinates and the magnitude of the point Q as functions of time are shown in Fig. 38.

The point Q reaches the maximum speed value of 24.986 mm/s at the middle of the stroke (21.5 mm), after 1.57 s from the lower position of the slide (Fig. 39).

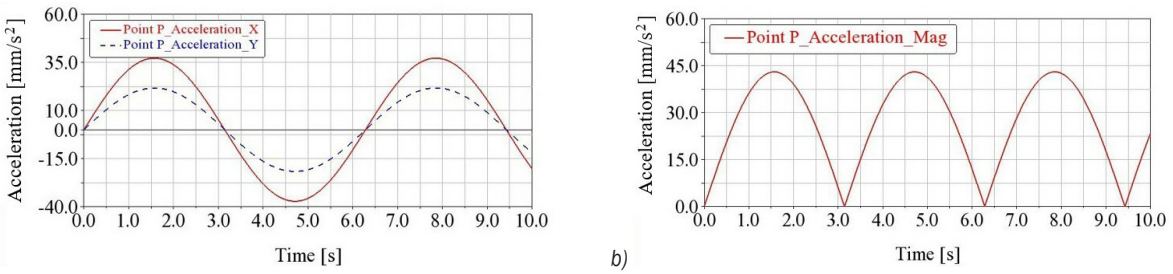

Fig. 37. *The diagram of acceleration for point* P*; a) the projections on the system axes, and b) the magnitude*

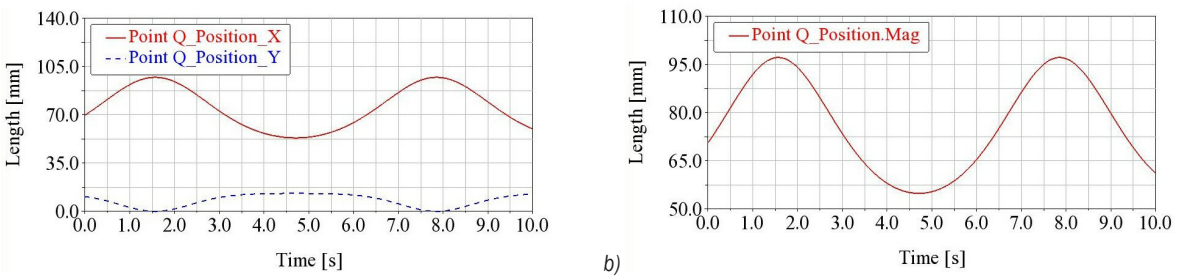

Fig. 38. *The diagram of coordinates for point* Q*: a) the Cartesian coordinates, and b) the polar radius*

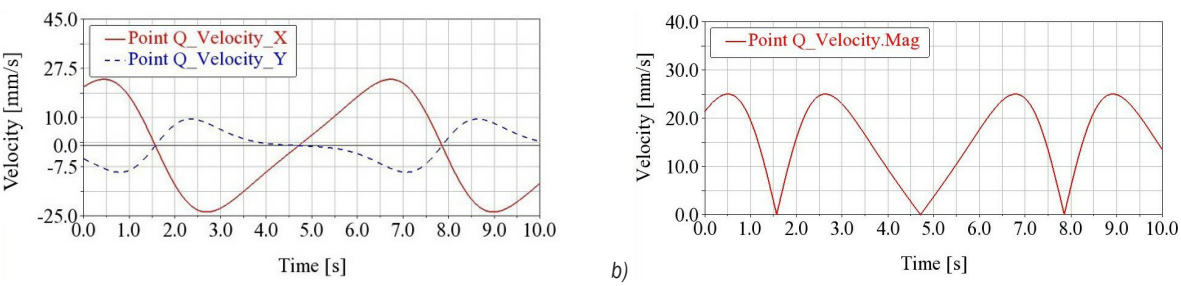

Fig. 39. *The diagram of velocity for point Q: a) the projections on the system axes, and b) the magnitude*

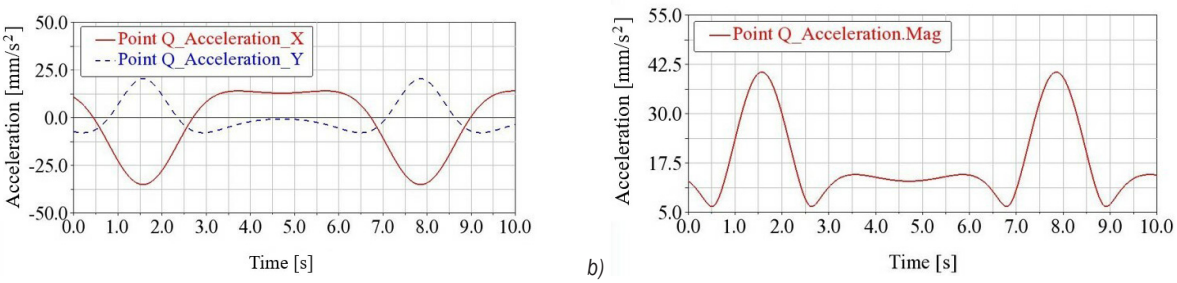

Fig. 40. *The diagram of acceleration for point Q; a) the projections on the system axes, and b) the magnitude*

The acceleration has three local maxima (40.532 mm/s^2, 14.557 mm/s^2 and 14.557 mm/s^2) on a double stroke (Fig. 40).

2.3 Elliptical Direct Curve

The case when the direct curve of P is an ellipse has also been studied. An ellipsograph mechanism was taken into consideration (Fig. 41); the points on the GH connecting rod describe ellipses, if one of the slides is the driving element.

Artobolevsky's mechanism from Fig. 11 to which the ellipsograph mechanism is joined was considered so that the initial curve is an ellipse. The kinematic scheme for this adapted mechanism is given in Fig. 42.

The following dimensions were used for this mechanism: $x_F = 100$ mm, GH = 79 mm, GP = 36 mm,

AB = 100 mm. If the slide 8 is the driving element, the coordinate x_G at a given time is known.

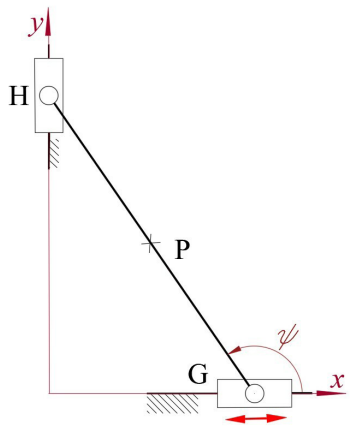

Fig. 41. *The ellipsograph mechanism*

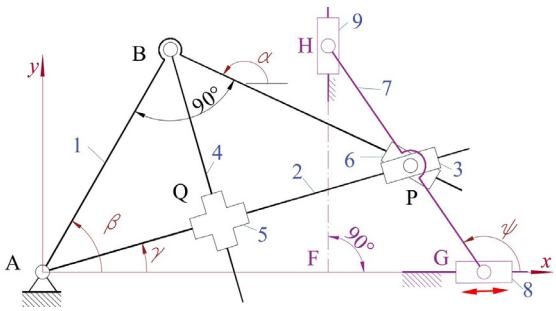

Fig. 42. *The kinematic scheme of the mechanism*

Eqs. (25) to (28) are useful for the calculus of Cartesian coordinates of H and P points.

$$x_H = x_G + GH\cos\psi = x_F = \text{const.}, \tag{25}$$

$$y_H = y_G + GH\sin\psi, \tag{26}$$

$$x_P = x_G + GP\cos\psi, \tag{27}$$

$$y_P = y_G + GP\sin\psi. \tag{28}$$

A simulation was performed with the GWBASIC® program, the driving element 8 having a constant velocity; the mechanism in one position is given in Fig. 43, and some successive positions of it are depicted in Fig. 44.

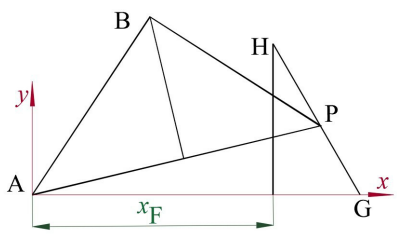

Fig. 43. *The mechanism in one position*

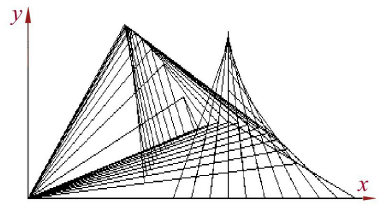

Fig. 44. *The mechanism in a few successive positions*

The curve drawn by point P during simulation is only a part of an ellipse (Fig. 45), being limited by the points of intersection P_1 and P_2, between the circle drawn by point B and the ellipse drawn by point P, due to the geometry of the mechanism (Fig. 46).

Fig. 45. *The curve drawn by point* P *(GWBASIC® program)*

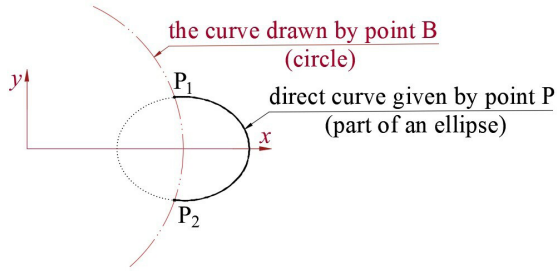

Fig. 46. *The limitation of the mechanism functioning*

The Cartesian coordinates of points P_1 and P_2 were determined with the Maple® software by solving Eq. (29).

$$\begin{cases} x^2 + y^2 = R^2 \\ \dfrac{(x-R)^2}{a^2} + \dfrac{y^2}{b^2} = 1 \end{cases}, \tag{29}$$

where R = AB = 100 mm, a = PH = 43 mm and b = PG = 36 mm.

The values of the coordinates of the locking points resulted as follows: $x_{P1} = x_{P2} = 93.4559$ mm, $y_{P1} = -y_{P2} = 35.5806$ mm.

To avoid the blockage in the operation of the mechanism, the abscissa of point F must be greater than the sum of the dimensions AB and HP. The inverse curve obtained during simulation is that of Fig. 47.

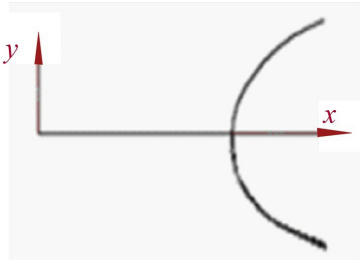

Fig. 47. *The inverse curve drawn by point Q (GWBASIC® software)*

The geometrical model of the mechanism was obtained with the SolidWorks® software and imported into the ADAMS® software for the kinematic analysis (Fig. 48). The starting position of the mechanism was considered in x_G = 137.79 mm and the corresponding coordinates of the point P are x_{P0} = 120.57 mm and y_{P0} = 31.613 mm (near to the point P_1).

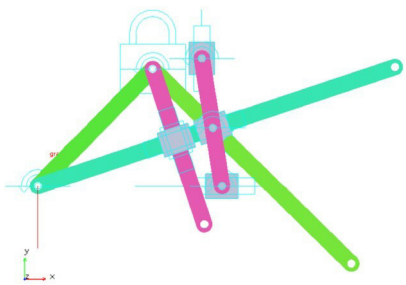

Fig. 48. *The model of the mechanism in the ADAMS® software*

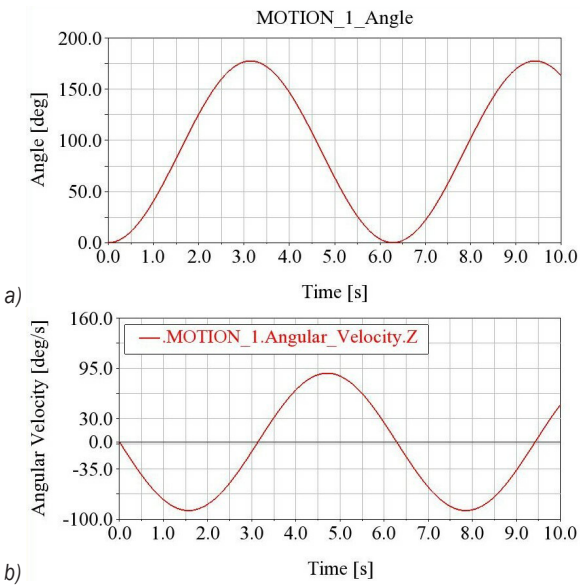

Fig. 49. *Motor kinematic diagrams; a) the angle, and b) angular velocity*

The engine from the G-rotation joint has the motion law given by Eq. 30. In the ADAMS® software the option "*velocity*" is selected.

$$f\left(time\right)=1.55\cdot\sin\left(time\right). \tag{30}$$

The maximum angular velocity of the engine is 85.94 deg/s (Fig. 49b) and the angular stroke of it is 171.88 degrees (Fig. 49a).

The Fig. 50 shows the elliptical curves generated by points P and Q using the ADAMS® software.

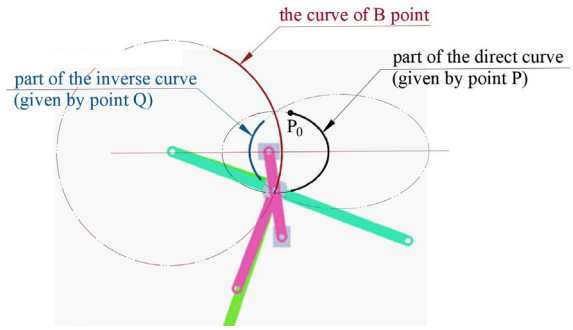

Fig. 50. *The curves drawn in the ADAMS® software*

The diagrams of the Cartesian coordinates and the polar radius of the point P as functions of time are shown in Fig. 51.

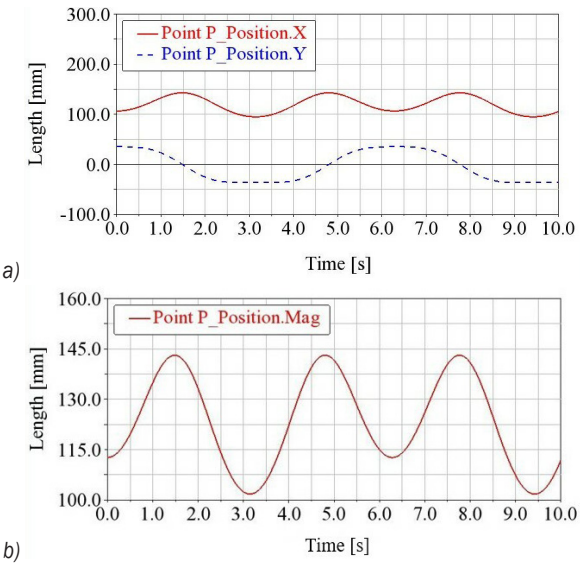

Fig. 51. *The diagram of coordinates for point* P*; a) the Cartesian coordinates, b) the polar radius*

For the selected 2×171.88 degrees double angular stroke of the motor, the point P will have an oscillating motion on an elliptical trajectory. When the point P moves clockwise on the ellipse (Fig. 51), the point Q moves in the trigonometric direction on its ellipse (Fig. 54).

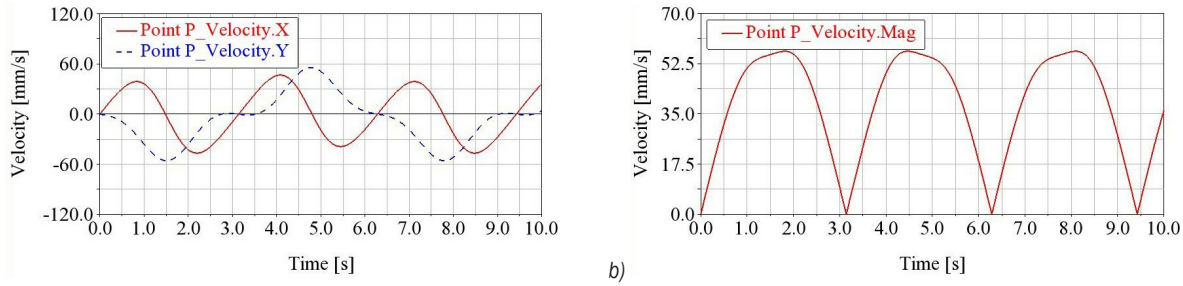

Fig. 52. *The diagram of velocity for point* P*; a) the projections on the system axes, and b) the magnitude*

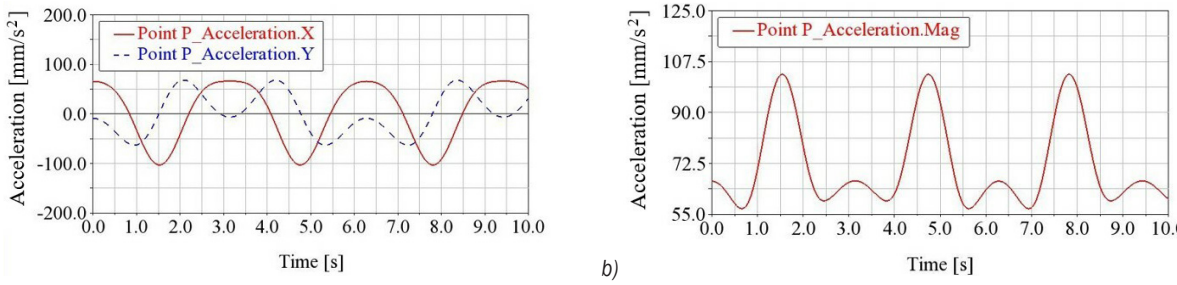

Fig. 53. *The diagram of acceleration for point* P*; a) the projections on the system axes, and b) the magnitude*

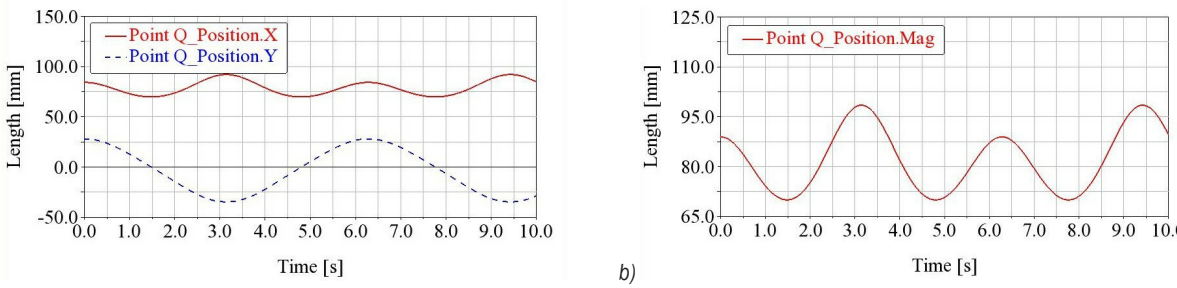

Fig. 54. *The diagram of coordinates for point* Q*; a) the Cartesian coordinates, and b) the polar radius*

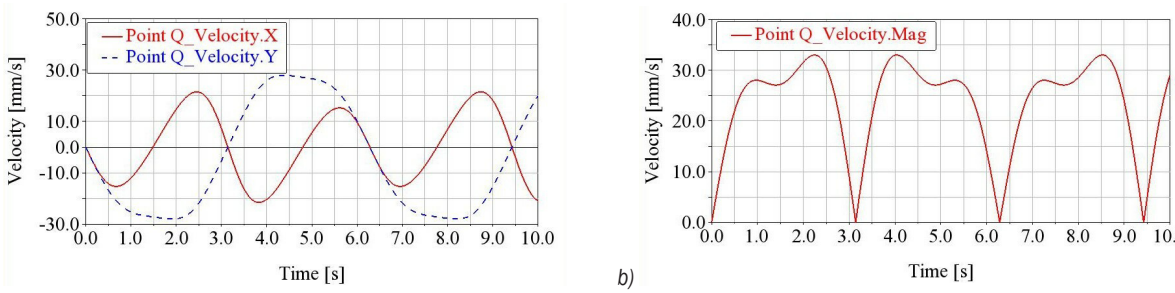

Fig. 55. *The diagram of velocity for point* Q*; a) the projections on the system axes, and b) the magnitude*

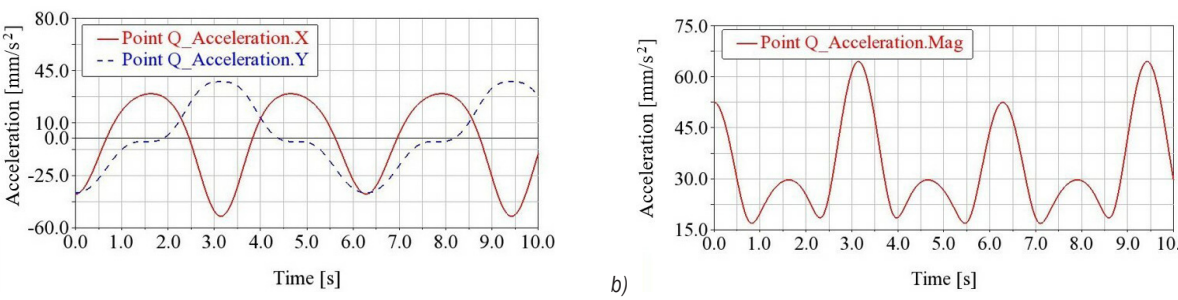

Fig. 56. *The diagram of acceleration for point* Q*; a) the projections on the system axes, and b) the magnitude*

The inverse curve drawn by the point Q is also an ellipse but the maximum velocity of point Q (Fig. 55) is slower than that of point P (33.2 mm/s and 57.5 mm/s, respectively) (Fig. 52) and the maximum acceleration of point Q also has lower values (65 mm/s^2 and 103.12 mm/s^2, respectively) (Fig. 56) than that of point P (Fig. 53).

2.4 Spiral direct curve

The case in which point P describes an Archimedes' spiral was also analysed. The proposed mechanism has the kinematic scheme given in Fig. 57. In order to have the point P drawing the Archimedes' spiral, two motors were used: one in rotation joint F and one in translation joint P (8,7), with constant angular velocity and constant linear velocity respectively.

The equation of an Archimedes' spiral drawn by point P is $\rho = a \cdot \varphi$, where a is a constant and φ and ρ are their polar coordinates in relation to the fixed system xFy_1.

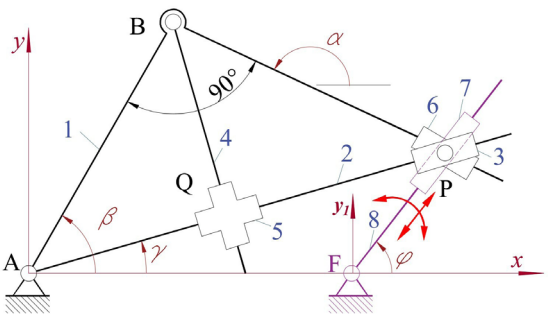

Fig. 57. *The kinematic scheme of the mechanism*

The following input data were considered for this mechanism: x_F = 100 mm, AB = 100 mm, a = 5 mm and φ = 0 to 4π.

The direct and inverse curve obtained with the GWBASIC® software are presented in Figs. 58 and 59.

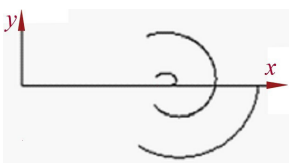

Fig. 58. *Divided Archimedes' spiral drawn by point P*

Fig. 59. *The inverse curve, described by point Q*

For the functioning of the mechanism on the three sub-intervals (Fig. 60), the element 8 must be positioned at one end of each divided curve.

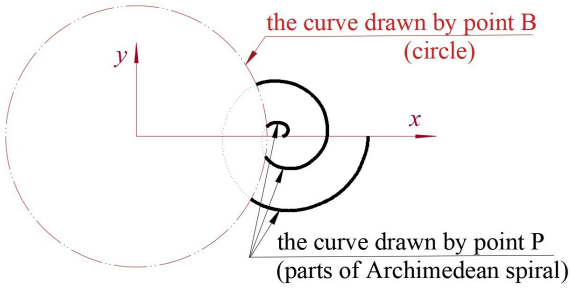

Fig. 60. *The limitation of the operating area*

The mechanism does not work in two sub-intervals and the limiting points are found at the intersection between the curve described by point B and that described by point P (Fig. 60).

The limitation of the operating area depends on the geometry of the mechanism and on the velocities of the two motors. If other values for the velocities of the motors are adopted, the pitch of the spiral will be changed. If the pitch is too large, the spiral drawn on the first 360 degrees will not intersect the circle generated by point B. For example, for the velocity of the linear motor of 30 mm/s and angular velocity of the rotary motor 0.6 rad/s, the constant of the Archimedes' spiral a = 50 and its pitch of 314.16 mm are obtained and the mechanism does not lock.

If one intends to keep the shape of a spiral that intersects the circle of B, the abscissa of point F must be increased, such as to avoid the functioning limitation. The geometrical model of the mechanism was obtained with the SolidWorks® software and imported into the ADAMS® software for the kinematic analysis (Fig. 61).

Two motors were placed in the ADAMS® software: one rotary in F joint and one linear in P-translation joint (7, 8).

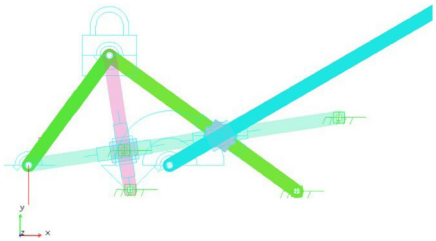

Fig. 61. *The model of the mechanism in the ADAMS® software*

In the case in which the point P goes on the direct curve in trigonometric direction with the angular

velocity of the driving element of 0.6 rad/s and the linear motor speed of 2 mm/s, the curves from Fig. 62 are obtained.

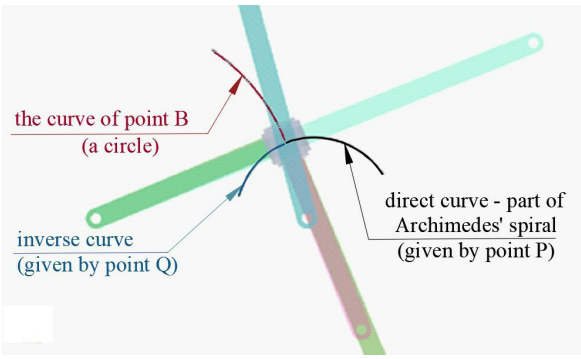

Fig. 62. *The case for trigonometric direction of* P *point motion*

Fig. 63 depicts the curves obtained when the point P goes on the direct curve in clockwise direction, with the angular velocity of the driving element of –0.6 rad/s and the linear motor speed of –2 mm/s.

The values of engine velocities determine the equation of the Archimedes' spiral (Eqs. (31) and (32)). $a = 3.33$ mm and the pitch of Archimedes' spiral equals 20.94 mm.

$$\rho = a \cdot \varphi, \tag{31}$$

$$\dot{\rho} = a \cdot \dot{\varphi}. \tag{32}$$

The position kinematic diagrams for point P are shown in Fig. 64 for this case.

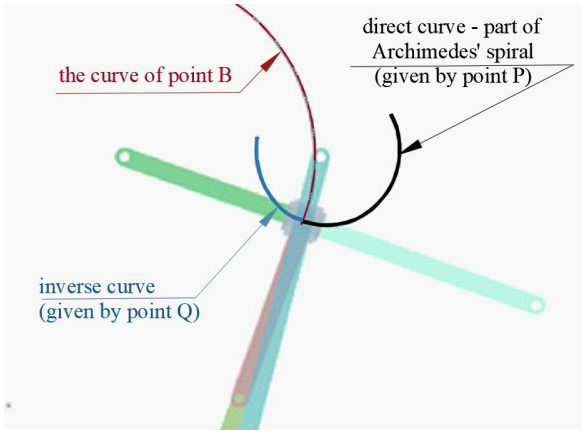

Fig. 63. *The case for the clockwise direction of* P *point motion*

During the functioning interval of 4 s, the slide 7 is moved with constant velocity by the linear motor towards the rotation joint C, but the velocity tangential component of the point P imposed by rotation motor decreases due to the decreasing of the radius, so that the absolute velocity diagram of the point is descending (Fig. 65).

Although the slope of the velocity diagram is constant, the acceleration is variable (Fig. 66) because the normal acceleration depends on the polar radius

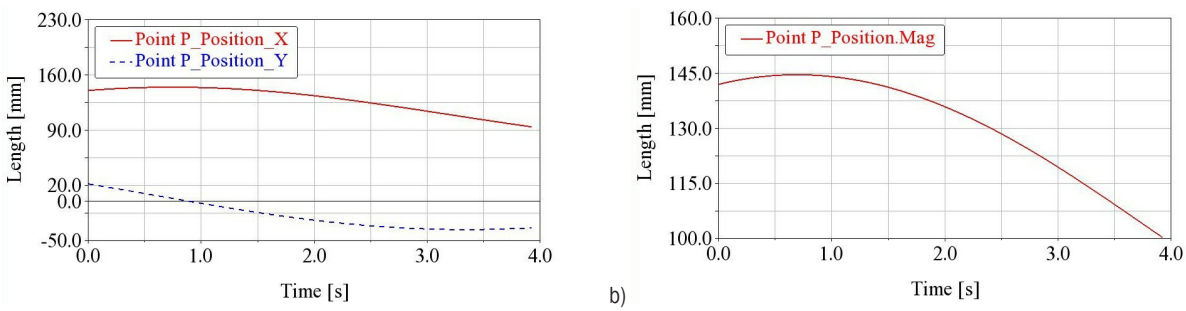

a) b)

Fig. 64. *The diagram of coordinates for point* P*; a) the Cartesian coordinate on* x_{Ay} *system, b) the polar radius*

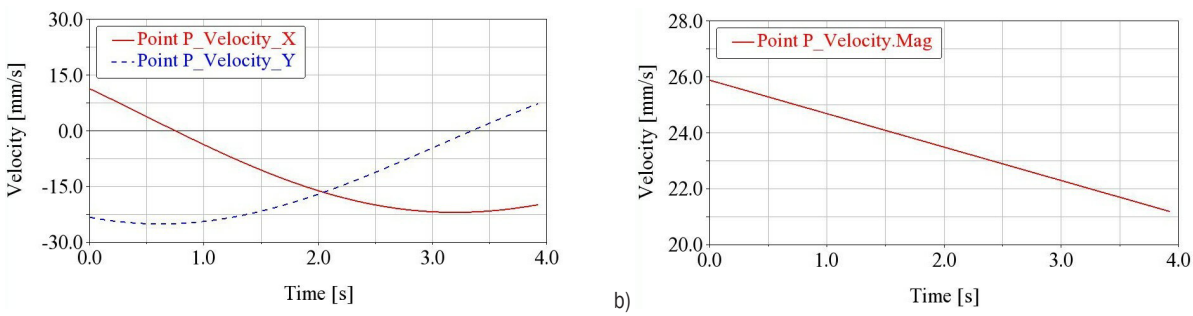

a) b)

Fig. 65. *The diagram of velocity for point* P*; a) the projections on the system axes, and b) the magnitude*

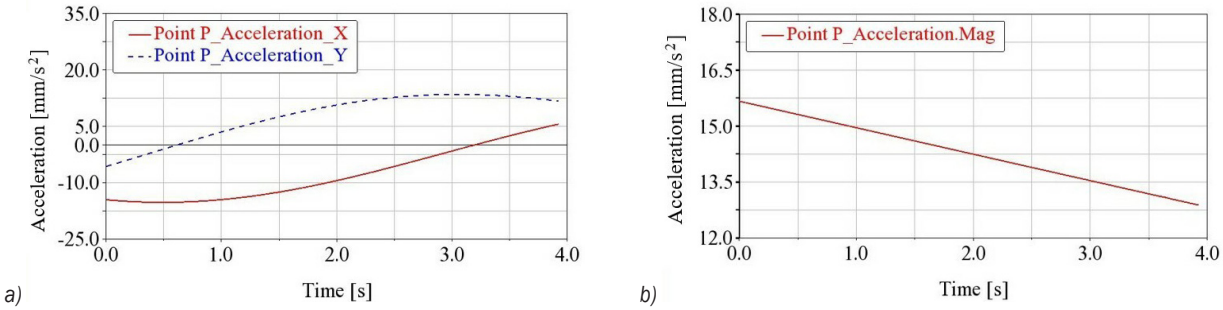

a) b)

Fig. 66. *The diagram of acceleration for point* P; *a) the projections on the system axes, and b) the magnitude*

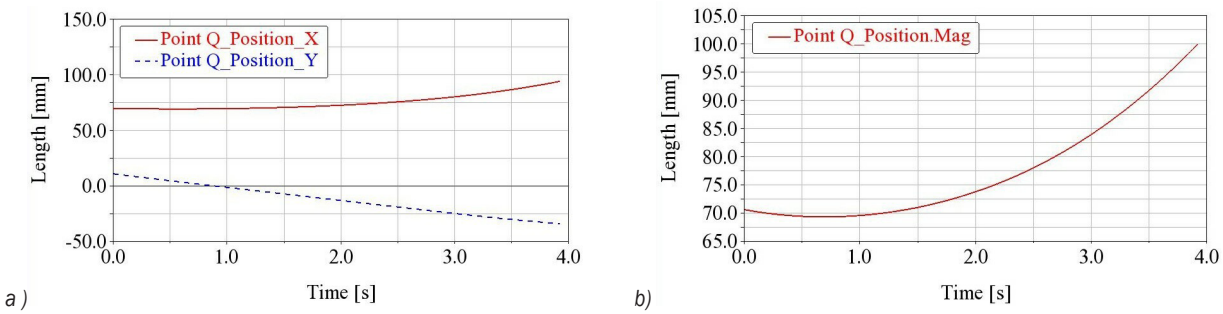

a) b)

Fig. 67. *The diagram of coordinates for point* Q; *a) the Cartesian coordinates, ad b) the magnitude*

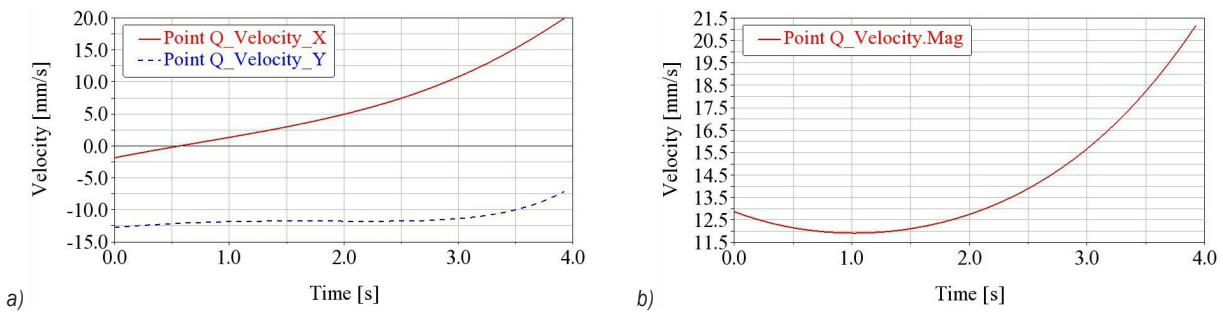

a) b)

Fig. 68. *The diagram of velocity for point* Q; *a) the projections on the system axes, b) the magnitude*

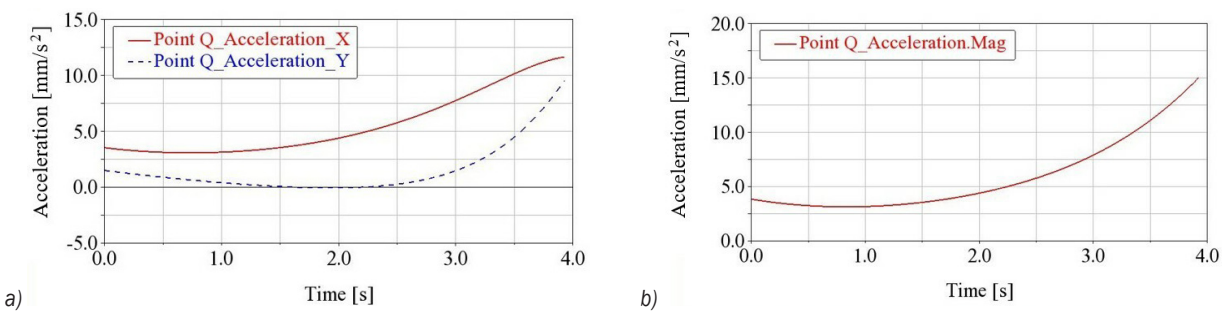

a) b)

Fig. 69. *The diagram of acceleration for point* Q; *a) the projections on the system axes, and b) the magnitude*

of the point P. In the initial position, the point P has the polar radius of 43 mm referring to the xFy_1 system and the normal acceleration is a^n = 15.48 mm/s², according to the kinematic diagram.

The animation and diagrams of the velocities reveal that the point P moves on the direct curve in a clockwise direction and the point Q goes in trigonometric direction on the inverse curve (Figs. 65 and 68).

While the velocity magnitude of the tracer point P of the direct curve is decreasing, that of the tracer point of the inverse curve is decreasing in the first phase and is increasing in the second phase to the value of 21 mm/s (Fig. 67).

The diagram of acceleration magnitude for point Q is shown in Fig. 69b and its maximum value is 15 mm/s^2 at the end of the interval.

3 CONCLUSIONS

This work has brought attention to the creation of new inversor mechanisms that draw exactly imposed curves and has analysed their functioning. We have established some applications for the inversor mechanisms in lifting-lowering systems, conveyor belts, machine tools, curve generation mechanisms, kinetic light art, and other industrial mechanisms.

A Crawford inversor mechanism has been analysed, and we have concluded that it is suitable for rapid placement/retraction movements in/from a given position of an object. It is also possible to perform optimization in order to coordinate the operating time.

Four new inversor mechanisms have been designed, starting from the structure of Artobolevsky's inversor mechanism, by adding kinematic chains that draw different direct curves (a circle, a straight line, an ellipse, and an Archimedean spiral).

Kinematic analysis of all these mechanisms was performed and the obtained inverse curves are in accordance with the information from **[3]**.

Following the results obtained for the proposed mechanisms, conclusions were drawn to avoid blockage in each particular studied case. The avoidance of the locking is achieved by modifying the geometry of the mechanisms, and for the case of the direct Archimedean spiral curve this can also be done by modifying the motion parameters of the motors.

We emphasise that the premises for a full motion study, including dynamic one, have been created for inversor mechanisms.

4 ACKNOWLEDGEMENTS

This research received no specific grant from any funding agency in the public, commercial, or not-for-profit sectors.

The authors declare that they have no conflict of interest.

5 REFERENCES

[1] Taimina, D. (2007). Historical mechanisms for drawing curves. Amy Shell-Gellasch, (ed.) *Hands on History: A Resource for Teaching Mathematics*, p. 89-104, Mathematical Association of America, **DOI:10.5948/UP09780883859766.011**.

[2] Brix, T., Döring, U., Reeßing, M. (2011). Creating Present-Day Solutions from Historical Knowledge. *13th World Congress in Mechanism and Machine Science*, p. 1744-1751.

[3] Weisstein, E.W. (2020). Inverse Curve, from MathWorld - A Wolfram Web Resource. from *https://mathworld.wolfram.com/InverseCurve.html*, accessed on 2020-05-10.

[4] Steiner, J. (2020). Encyclopedia Britannica, no. 1911, from *https://en.wikisource.org/wiki/1911_Encyclop%C3%A6dia_Britannica/Steiner,_Jakob*, accessed on 2020-05-10.

[5] Artobolevsky, I.I. (1959). *Mechanism theory for solving planar curve problems*. Academy of Sciences of the USSR, Moscow. (In Russian).

[6] Tienari, O. (1980). *Reversing mechanism for the direction of rotation in a drilling apparatus*. Patent US4399876A, United States Patent Office, Washington.

[7] Artobolevsky, I. (1975). Mechanisms in Modern Engineering Design: A Handbook for Engineers, Designers and Inventors, from *https://archive.org/details/mechanism_in_modern_engineering_V1-lever_mechanism*, accessed on 2020-05-10.

[8] Bullough, W.A., Johnson, A.R., Makin, J., Tozer, R.C. (2001). ESF Clutch Driven Mechanisms and the ER Linear Inversor Motion a Demonstrator. Sulejman, A. (ed.) *Smart Structures*, vol. 429, Springer, Vienna, **DOI:10.1007/978-3-7091-2686-8_14**.

[9] Duca, C.D.; Buium, F., Pârăoaru, G. (2003). *Mechanisms*, Gh. Asachi, Iaşi. (In Romanian)

[10] Artobolevsky, I.I. (1971). *Mechanism in Modern Technology*. Vol. II., Nauka, Moscow. (In Russian)

[11] Tutunaru, D. (1969). *Planar Rectilinear Mechanisms and Inversor Mechanisms*. Tehnica, Bucharest. (In Romanian)

[12] Chalfin, N.L. (1961). *Phonograph Pickup Arm*. Patent 2977126A, United States Patent Office, Washington.

[13] Garrec, P. (1993). *Device for Transmitting Movement between a Solid and a Member, in Particular for a Robot Able to be Moved on Legs*. Patent 5219410 A, United States Patent Office, Washington.

[14] Kunzler, P.A., Schmitt, P., Poblano, R.D.V., Chan, B., Liang, P.A., Vairani, F.H., Kilian, A., Chin, R.C., Mitchell, W.J. (2011). *Wheel Embedded Suspension*. Patent 7938210B2, United States Patent Office, Washington.

[15] Nickstadt, G. (1974). *Gear Drive Reversing Mechanism*, Patent US3851537A, United States Patent Office, Washington.

[16] Shkolnik, N. (1984). *Walking Apparatus*. Patent US4462476A, United States Patent Office, Washington.

[17] Stephenson valve gear. Wikipedia, from *https://en.wikipedia.org/wiki/Stephenson_valve_gear*, accessed on 2020-05-10.

[18] Dijksman, E.A. (1994). True straight-line linkages having a rectilinear translating bar. Lenarčič, J., Ravani, B. (eds). *Advances in Robot Kinematics and Computational Geometry*, p. 411-420, Springer, Dordrecht, **DOI:10.1007/978-94-015-8348-0_41**.

[19] Evert, A., Dijksman (1993). A way to generalize Peaucellier's inversor. *The 6th IFToMM International Symposium on Linkages and Computer Aided Design Methods*, vol. 1, p. 73-82.

[20] Halicioglu, R., Dulger, L.C., Bozdana, A.T. (2014). Modelling and simulation based on Matlab/Simulink: A press mechanism. *2nd International Conference on Mathematical Modeling in Physical Sciences, Journal of Physics: Conference Series*, vol. 490, art. ID 012053, **DOI:10.1088/1742-6596/490/1/012053**.

[21] Tavoleri, C., Ottaviano, E., Ceccarelli, M. (2007). Design and problems of a new leg-wheel walking robot. *Advances in Climbing and Walking Robots. Proceedings of 10th International Conference*, p. 319-328, **DOI:10.1142/9789812770189_0038**.

[22] Simionescu, P.A; Tempea, I. (1999). Kinematic and kinetostatic simulation of a leg mechanism, *10th World Congress on Theory of Machines and Mechanisms*, p. 572-576.

[23] Halicioglu, R., Dulger, L.C., Bozdana, A.T. (2017). An automation system for data processing and motion generation. *International Artificial Intelligence and Data Processing Symposium*, **DOI:10.1109/IDAP.2017.8090294**.

[24] Nunez-Altamirano, D.A., Juarez-Campos, I., Márquez-Pérez, L., Flores-Díaz, O., Romero-Munoz, L. (2016). Dynamics of a novel robotic leg based on the Peaucellier - Lipkin mechanism on linear paths during the transfer phase. *Advances in Mechanical Engineering, Advances in Mechanical Engineering*, vol. 8, no. 7 p. 1-10, **DOI:10.1177/1687814016657046**.

[25] Huang, M. (2019). On dimension synthesis of Hart's inversor III straight-line mechanism as a precision robotic end-of-arm tool. *Proceedings of ASME International Mechanical Engineering Congress and Exposition, Volume 4: Dynamics, Vibration, and Control,* **DOI:10.1115/IMECE2019-11522**.

[26] Kawamoto, A. (2004). *Generation of Articulated Mechanisms by Optimization Techniques*. PhD thesis, Technical University of Denmark, Lyngby.

[27] Zhu, B., Zhang, X., Zhang, H., Liang, J., Zang, H., Li, H., Wang, R. (2020). Design of compliant mechanisms using continuum topology optimization: A review. *Mechanism and Machine Theory*, vol. 143, art. ID 103622, **DOI:10.1016/j.mechmachtheory.2019.103622**.

[28] Halicioglu, R., Jomartov, A., Kuatova, M. (2021). Optimum design and analysis of a novel planar eight-bar linkage mechanism. *Mechanics Based Design of Structures and Machines*, **DOI:10.1080/15397734.2021.1995410**.

[29] Tuleshov, A., Halicioglu, R., Shadymanova, A., Kuatova, M. (2021). Kinematic synthesis method and eccentricity effects of a Stephenson mechanism. *Mechanical Science*, no. 12, p. 1-8, **DOI:10.5194/ms-12-1-2021**.

[30] Ahrendt, M.H. (1944). A general method for the construction of a mechanical inversor. *Mathematics Teacher,* vol. 37, no. 2, p. 75-80, **DOI:10.5951/MT.37.2.0075**.

[31] Bryant, J., Sagwin, C. (2008). *How round is your circle? When engineering and mathematics meet.* Princeton University Press, Princeton.

[32] Juarez-Campos, I., Nunez-Altamirano, D., Marquez-Perez, L., Romero-Munoz, L., Juarez-Campos, B. (2018). Hexapod with legs based on Peaucellier-Lipkin mechanisms: A mathematical structure used in reconfiguration for path planning. *International Journal of Advanced Robotic Systems*, p. 1-18, **DOI:10.1177/1729881418795929**.

[33] Zhan, J.; Yang, K.; Huang, Z. (2014). Topological design of hinge-free compliant mechanisms using the node design variables methods. - In: Zhang, X., Liu, H., Chen, Z., Wang, N. (eds.) *Intelligent Robotics and Applications. Lecture Notes in Computer Science*, vol 8918. Springer, Cham, p. 567-575, **DOI:10.1007/978-3-319-13963-0_57**.

[34] Schoofs, I. (2020). Mesmerizing Slow Motion, from *https://ivoschoofs.com/project/just-because-you-are-a-character-doesnt-mean-you-have-character/*, accessed on 2020-05-10.

[35] Buckley, J., Huang, M.Z. (2011). A study on dimension synthesis for the peaucellier mechanism. *Proceedings of ASME International Mechanical Engineering Congress and Exposition*, **DOI:10.1115/IMECE2011-64278**.

[36] Crawford, W.R. (1936). The mechanical construction of the general conic section. *Engineer*, vol. 162, no. 4207.

[37] An Ingenious Reversing Mechanism for Machine Tools (1899). Scientific American, from *https://www.scientificamerican.com/article/an-ingenious-reversing-mechanism-fo/*, accessed on 2020-05-10.

[38] Gogu, G. (2005). Mobility of mechanisms: a critical review. *Mechanism and Machine Theory*, vol. 40, no. 9, p. 1068-1097, **DOI:10.1016/j.mechmachtheory.2004.12.014**.